JOURNAL OF COMPUTATIONAL PHYSICS **130,** 243–255 (1997)
ARTICLE NO. CP965582

An Inverse Finite Element Method for Pure and Binary Solidification Problems

Alexandre I. Fedoseyev[1] and J. Iwan D. Alexander

Center for Microgravity and Materials Research, University of Alabama in Huntsville, Huntsville, Alabama 35899

Received September 18, 1995; revised July 9, 1996

A 2D axisymmetric formulation for the solution of a directional solidification problem using an inverse finite-element method (IFEM) is presented. An algorithm developed by A. N. Alexandrou (*Int. J. Numer. Methods Eng.* **28,** 2383, 1989) has been modified and extended to include more general boundary conditions. The latter includes the explicit presence of an ampoule (with a complex shape) that contains the solid and the melt from which it is growing. Heat transfer between the ampoule and the external environment, time-dependent thermal boundary conditions, nonmonotonic temperature distributions, and species diffusion in the melt and crystal are also taken into account. Thus, our extended formulation encompasses a wider class of solidification problems than previous IFEM methods. Numerical experiments that illustrate the suitability of the extended IFEM are presented. In particular, we present a simulation of the directional solidification of zinc cadmium telluride using boundary conditions corresponding to an actual experiment scenario.

1. INTRODUCTION

Phase change free boundary problems related to solidification or melting represent a class of problems that require simultaneous solution of the governing partial differential equations and the geometry of the domain on which they are defined. Solution techniques for such problems include coordinate transformation techniques, enthalpy methods, inverse formulation methods, phase field models and, more recently, the inverse finite-element method (IFEM). All these methods, have, in one form or another, been applied to the problem of the directional solidification of pure substances and binary compounds (see [1]). Directional solidification is a commonly used technique for the production of semiconductor crystals and some metal alloys. Essentially, the solid, usually a crystal, is grown by translating a melt relative to an imposed temperature gradient such that it gradually freezes in the direction antiparallel to the translation direction (see Fig. 1).

The existing solution techniques for such problems can be subdivided into the following classes:

(a) *Coordinate transformation techniques.* Here the unknown is mapped onto a regular geometrical region. The resulting transformed equations are then solved on this domain using $N - 1$ of the N boundary conditions. The Nth condition, sometimes referred to as the *distinguished* condition [1] is used to determine the location of the free or moving boundary in physical space in an iterative fashion. This approach has been realized, using different solution techniques, including finite element [2–5] and, recently, Chebyshev spectral techniques [6]. The techniques employed to handle the mapping include Landau-type transformations [6, 7] and numerically generated moving orthogonal curvilinear systems obtained by elliptic mesh generation methods (see, for example, [8]).

(b) *Enthalpy methods.* Enthalpy methods, first suggested by Rose [9], are "fixed domain" based approaches to phase change problems which do not require explicit tracking of the phase boundary. The method involves casting the energy transport equation in conservation form [10] and defining an enthalpy function for the entire two-phase domain. As solidification proceeds, the location of the boundary between the solid and liquid phases is then determined from the enthalpy distribution and the fraction of solid or liquid occupying each cell. These techniques have been applied successfully to solidification problems for pure substances and binary compounds (see, for example, [10–14]).

(c) *Phase field models.* The phase-field approach involves the assumption that a phase-field $\phi(\boldsymbol{x}, t)$ exists which specifies the phase of the system at each point $\boldsymbol{x}$. It is then assumed that the total Helmholtz free energy of the system, F, is a functional dependent on ϕ, temperature, composition, etc. The dependence of F on ϕ is assumed to be of a "double well" form [15] and is usually taken in the form of an explicit dependence on local gradients of ϕ. The different models that are based on the phase field ideas are reviewed by Hohenberg and Halperin [16] and, for solidification in particular, have been developed by Langer [17] and Caginalp [18]. Various studies performed using this approach have shown that it can successfully reproduce

[1] On leave from the Institute for Problems in Mechanics, Russian Academy of Sciences, 101 Vernadsky Av, Moscow, Russia, 117526.

0021-9991/97 $25.00

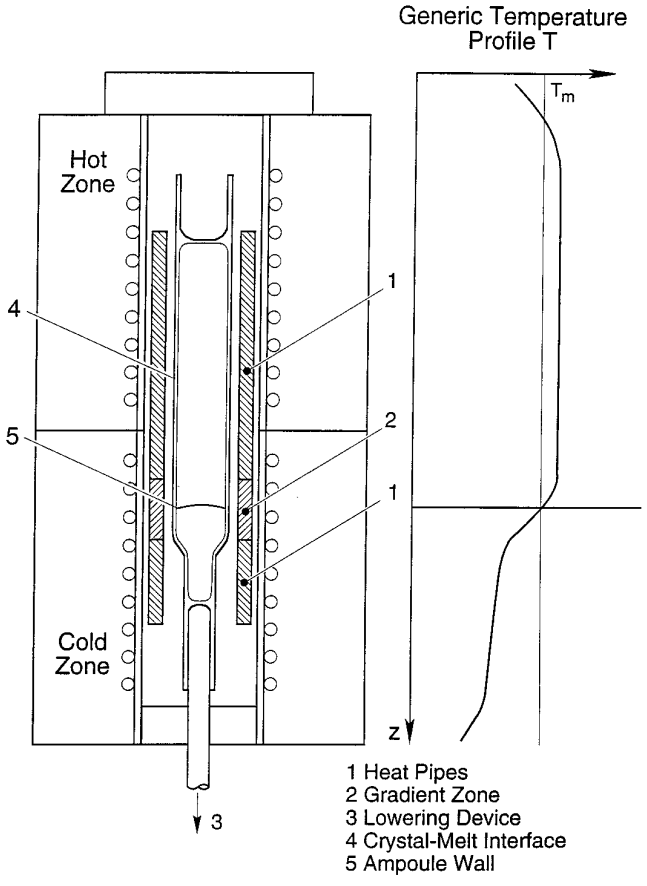

FIG. 1. Physical model of the directional solidification technique.

complex solid–liquid interface shapes associated with solidification of a pure material [19–21].

(d) *Inverse methods.* For the approaches described in (a) and (b), the temperature field and the melt–liquid interface are taken to be unknown functions that depend on position, $\boldsymbol{x}$, and time, t. In contrast, for the inverse formulation, the positions, $\boldsymbol{x}$, are taken to be the unknowns [22]. The earliest inverse approaches achieved this by defining a set of orthogonal coordinates that are based on the orthogonality of isotherms and heat flow lines. The governing equations were then transformed accordingly so that temperature became the independent variable. The isotherm migration method was one of the earliest inverse methods to be successfully applied to solidification problems. It has recently been employed to study the effect of nonlinear radiation boundary conditions on temperature field kinetics [23, 24]. This particular inverse method is restricted to 1D or linear problems only since it is difficult to find the appropriate coordinate transformation for 2 and 3D nonlinear problems. An alternative inverse finite-element method (IFEM) for directly formulated free boundary problems has recently been proposed [25] which is not restricted to linear problems. In this approach, the temperatures are fixed at the mesh nodes. The mesh nodes are then moved such that the energy transport equations are satisfied at the new node locations. Thus, it differs from the previous inverse approach [22] in that the inverse transformation is not required. Thus, while the problem is inversely defined, it is not mathematically inverted.

The application of the previously developed IFEM method [25] to solidification problems is, in general, limited if the temperature field is complicated or the initial approximations are singular. In [25], the internal temperature field was required to be spatially monotonic in order to ensure the existence of solutions. However, as explained later, this restriction can be avoided if the Newton method used to update the mesh node locations is modified. We have extended the method to include time-dependent thermal boundary conditions. In practical applications, another limitation of previous IFEM approaches is that heat flow within the sidewalls is not considered. In fact, the container surrounding the melt and crystal was not considered at all. The requirement that the temperature field be spatially monotonic excluded the possibility of changing the boundary temperature (i.e., the melt-container temperature). Thus, the application to technologically interesting situations for which the finite extent of the ampoule or container must be treated explicitly was not possible. However, in problems for which the use of the ''quasi-steady approximation [26] is admissible, the monotonic temperature restriction need not be a problem. This is because, in the frame of reference used in this approximation, the ampoule wall temperatures do not change. Thus, provided one considers the solidification of a pure substance this causes no problems since, at least when interface kinetics are not important (i.e., the dependence of the interfacial temperature on the degree of undercooling) the melt–crystal interface will always be defined by a constant melting temperature. However, for situations in which interface kinetics are important, or where explicit dependence of melting temperature on curvature (Gibbs–Thomson effect) is considered, the IFEM method requires modification. For multicomponent systems where the melting temperature is composition dependent, the interface temperature will generally be nonuniform, regardless of whether kinetics or curvature-related effects are important. In such cases, the constraint that nodal temperature values remain fixed during the calculation must be relaxed if the IFEM method is to be applied.

In this paper we introduce an extension of the IFEM, described in [25], that allows the nodal temperatures to change and employs a more general mesh updating procedure than in previous applications. This extends the practical applications of IFEM to time-dependent boundary conditions, spatially nonmonotonic temperature fields and

the solidification of a binary alloy with a composition dependent melting temperature.

2. SOLIDIFICATION FROM A PURE MELT: FORMULATION

The problem of directional solidification involves either the translation of an ampoule through a furnace temperature profile (Bridgman technique [2, 5]; see Fig. 1) or modification of the furnace temperature profile with time (e.g., gradient freeze [27]). In both cases a fixed point on the ampoule wall will experience a change in a temperature with time that results in the directional solidification of the melt initially contained within the ampoule. The instantaneous position of the solidification front is determined by the temperature distribution inside the ampoule and the location of the melting temperature. For a pure substance, this is taken to be a constant and corresponds to an isotherm.

In the following formulation a general cylindrical coordinate system is employed, and vector $\boldsymbol{x} = (z, r)$ is referenced to points located inside the domain $\Omega = \Omega_c \cup \Omega_m$ or on the boundaries S_i (see Fig. 2).

In the absence of natural or forced convection in the melt and radiation, the governing equation for the temperature field is

$$c_p \rho \frac{\partial T}{\partial t} = \nabla(\lambda \nabla T) + Q \tag{1}$$

for $\boldsymbol{x} \in \Omega$, with applied boundary conditions

$$T = T_k(\boldsymbol{x}, t) \quad \text{for } \boldsymbol{x} \in S_k, k = 1, 3, ..., \tag{2}$$

and

$$-\lambda \frac{\partial T}{\partial n} = \alpha [T - T_{\text{ex}}(\boldsymbol{z}, t)] \quad \text{for } \boldsymbol{x} \in S_2, \tag{3}$$

where T is the temperature, Q is a heat source, ρ is the mass density which we take to the same for the solid and liquid,[2] $c_p = c_p(x)$ is the specific heat, and $S_1 \cup S_2 \cdots \cup S_k = S$ is the boundary of the region Ω, which includes ampoule, crystal, and melt. T_k is the temperature applied to the S_k boundary, α is a heat transfer coefficient, and $T_{\text{ex}} = T_{\text{ex}}(\boldsymbol{z}, t)$ is an external temperature profile which provides heat to the ampoule walls. $\lambda = \lambda(\boldsymbol{x})$ represents the thermal conductivity of the materials. In general, λ is different in the melt, solid, and ampoule and, for anisotropic crystals [28] may be represented by a second rank tensor. In contrast to earlier inverse approaches, orthogonality of heat flux lines and isotherms is not a requirement of IFEM and the extensions developed here. Thus, it can be applied to problems for which the conductivity is represented by a second rank tensor.

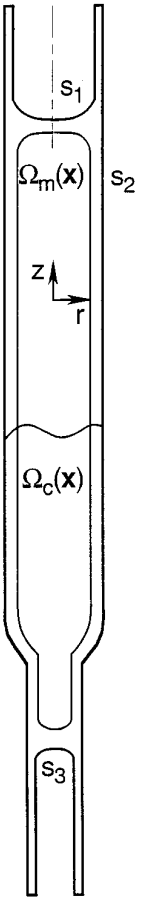

FIG. 2. Ampoule geometry, computational domain, and coordinate system.

The solidification front has no prescribed velocity. Its position and velocity must be determined from a global energy balance. Since a local energy balance must also be maintained, the conditions at the interface are

$$\rho L \boldsymbol{V} \cdot \boldsymbol{n} = \lambda_c \nabla T_c \cdot \boldsymbol{n} - \lambda_m \nabla T \cdot \boldsymbol{n} \quad \text{for } \boldsymbol{x} \in \Omega_m \cap \Omega_c, \tag{4}$$

$$T(\boldsymbol{x}, t) = T_m = T_c = T_{m0}, \quad \boldsymbol{x} \in \Omega_m \cap \Omega_c, \tag{5}$$

where L is the latent heat of solidification, $\boldsymbol{V}$ is the velocity of the melt–liquid interface, $\boldsymbol{n}$ is the outward pointing unit normal to the crystal along the solidification front, λ_c and λ_m are the thermal conductivities of crystal and melt, $\nabla T_c, \nabla T_m$, are the temperature gradients in the crystal and melt at the interface, T_{m0} is the melting temperature. Here it is assumed that the internal energy density is given by

[2] In practice this assumption is not always valid. However, depending on the particular situation, the technique presented here can be adapted for situations when the densities are different.

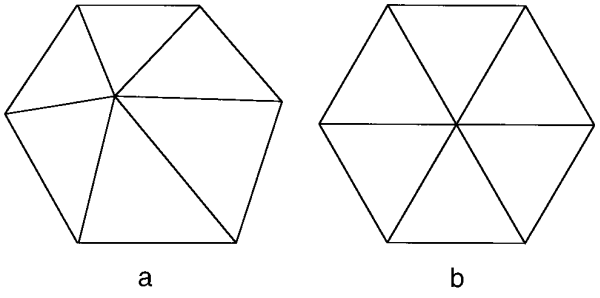

FIG. 3. Schematic showing the vertex averaging procedure operating on an irregular arrangement of triangular elements.

$e = c_p\, T$, where the specific heat, c_p, is taken to be constant over the range of temperatures considered.

3. IFEM SOLUTION METHOD

The solution of (1)–(5) starts from an initial estimate of the temperature field for a given set of points $\{\boldsymbol{x}_i\}$, which are represented by the mesh nodes. The $\{\boldsymbol{x}_i\}$ are determined by inverting (1)–(5) for a given applied temperature. This means that one fixes the temperature values at the nodes and finds the nodal positions. Equations (1)–(5) are implicit for $\{\boldsymbol{x}_i\}$ and nonlinear even in the simplest one-dimensional case; hence a Newton iterative solution technique is required. Details are provided below. The new $\{\boldsymbol{x}_i\}$ calculated at each time step redefine the spatial location of the isotherms such that the governing equations and all the boundary and interface conditions are satisfied. Thus, an implicitly inverse problem is defined. This method can be implemented using a finite-element method for rather general crystal–melt interface problems in complicated geometries.

The advantage of such an inverse approach is that the crystal–melt interface need not be tracked. It is located at the element boundaries and, thus, allows us to use a finite-element method (FEM) without any difficulty. The difference between the standard FEM method, and the inverse finite-element method (IFEM) is that the nodal values of the temperature field are taken to be fixed while the spatial position of these nodes is unknown. After an initial guess is made, the location of the nodes must be determined such that the temperature field satisfies the governing equations, boundary and interface conditions.

The approximation of the temperature field, $\boldsymbol{u}$, is taken in the form

$$\boldsymbol{u} = \sum_{i=1}^{N} u^i\, \Phi^i(x) \equiv u^i\, \Phi^i(x), \tag{6}$$

where $u^i = u^i(\mathrm{t})$ are the values of temperature in the N mesh nodes, and the $\Phi^i(\boldsymbol{x})$, $i = 1, ..., N$, are (linear or quadratic) basis functions. An implicit summation is made over repeated indices i in (6) and hereafter.

A Galerkin formulation is used to find the unknown node positions. As the position of the nodes change with time, the governing equation (1) is recast in the form

$$c_p \rho \left(\frac{\partial T}{\partial t} - V \cdot \nabla T \right) = \nabla(\lambda\, \nabla\, T) + Q, \tag{7}$$

where $\boldsymbol{V}$ is a nodal velocity. The corresponding Galerkin equations for (7) are then

$$\int_{\boldsymbol{G}} \left(c_p \rho \left(\frac{\partial u}{\partial t} - \boldsymbol{V} \cdot \nabla\, u \right) - \nabla(\lambda\, \nabla\, u) - Q \right) \Phi^i\, dG = 0, \quad i = 1, 2, ..., N. \tag{8}$$

A more detailed description of equation (8) is given in the Appendix.

Finite differences are used for time discretization. That is,

$$\frac{\partial u}{\partial t} = [u(t + \tau) - u(t)]/\tau, \tag{9}$$

where τ is the time step. An implicit solution scheme is used in time to avoid stability condition restrictions on the time step value τ. Each nodal velocity is computed from

$$\boldsymbol{V} = [x(t + \tau) - x(t)]/\tau. \tag{10}$$

Boundary conditions of the first kind are taken for the applied temperature (2) on the boundary S_k. This is implemented by fixing the node position in the algebraic system of equations. This means that the boundary location of mesh nodes with imposed temperatures remains unchanged. The crystal–melt interface, S_{m}, is characterized by a constant melting temperature, T_{m0}, and its location can be changed at each time step.

The adjustment of the crystal–melt interface location from time t to $t + \tau$ involves the following steps:

Step 1. Set the initial approximation for new nodal positions, including the interface nodes.

Step 2. Estimate the residual norm R of Eqs. (8).

Step 3. Change the position of the mesh nodes to decrease the nodal residuals R^i or stop iterations, if norm R is small enough.

Step 4. Return to step 2.

For quadratic convergence a Newton iterative technique is used in step 3,

$$x_i^{n+1} = x_i^n - \left(\frac{\partial R_i}{\partial x_j}\right)^{-1} R_j(x^n), \tag{11}$$

where $(\partial R_i/\partial x_j)^{-1}$ is the inverse of the Jacobian of the residuals R^j with respect to the location of the node x_j. The right-hand side of (11) uses values computed at the previous iteration. If the initial approximation is good enough, the convergence is rather fast.

Note that the number of equations in (8) is N, but to solve for the node positions requires that $2N$ values be given. This can be handled in different ways. For example, in [25] it is proposed to add N constraints to ensure orthogonality of the mesh. For conditions at fixed surfaces, like ampoule walls, this would require the use of elliptic mesh generation (EMG) to ensure orthogonality. In this paper an alternative approach is considered. It is less formal, robust and avoids the complexity that would arise with the use of EMG.

For the case of long cylindrical ampoules we need to change only the z-coordinate values of the mesh nodes. This means that the Jacobian in (11) involves only the "z"-derivative. The mesh node r-coorindate values are only moved (through a vertex averaging procedure described below) to satisfy the geometric constraints (that is, boundary nodes must remain on boundaries) and to maintain a smooth mesh distribution.

It should be noted that there are limitations to this technique. For example, internal temperature extrema will result in divergence of the inverse Jacobian in (11). Such extrema can be caused by internal heat sources or sinks or by time-dependent thermal boundary conditions. To treat problems with time-dependent boundary conditions we use the following approach:

Step 1.1. Set the initial approximation at the new time step t_{n+l} based on the solution at t_n. Smooth the mesh by some iterative procedure. We used a vertex averaging procedure. This shifts the nodes to the middle position relative to neighboring ones (see Fig. 3) and has a tendency to make the elements equilateral.

Step 1.2. Update nodal temperatures by solving (7). The crystal–melt interface temperature remains unchanged according to (5).

Step 2. Compute the residuals of Eq. (8).

Step 3. Update nodal positions to minimize the residual norm R. Process next time step (go to Step 1.1 of the algorithm), if R is small enough. In contrast to Step 1.1, where interface nodes are not moved, all nodes are moved. Boundary nodes on S_i, $i = 1, 2, ...$, are constrained to move along the appropriate boundary of S_i.

Step 4. Return to Step 2 for an additional Newton iteration, if R is not small enough.

In this way we again satisfy (1) but by changing temperature values at the mesh nodes and employing a two-step node position updating strategy. Such averaging procedures are sometimes used in conjunction with elliptic mesh generation techniques [29, 30] through the introduction of coordinate dependent weight functions. In these problems it prevents abrupt changes in mesh size and enables the generation of smoothly refined meshes.

For cases when internal heat sources cause local temperature extrema, the method will fail whenever the Jacobian in (11) is vanishingly small but the residual is finite.

4. COMPARISON WITH ANALYTICAL SOLUTION

To test the method, we solved a one-dimensional transient problem and compared the computed solution to an analytical one. The problem involves the penetration of a freezing front from a cold wall (temperature T_w) into an infinite melt. The melt is initially at the freezing temperature. This test problem has been proposed previously [25]. It is presented here for comparative purposes. For convenience we use a characteristic length L, $T_m - T_w$, and $L^2\rho c_p/\lambda$ to nondimensionalize length, temperature and time, and define $\theta = (T - T_m)/(T_m - T_w)$. This yields the following form of (7)

$$\frac{\partial \theta}{\partial t} = \frac{\partial^2 \theta}{\partial x^2}, \tag{12}$$

with boundary conditions $\theta(0, t) = -1$, for $t > 0$, the initial value $\theta(x, 0) = 0$, for $x > 0$; $\theta_m = 0$ and at the interface

$$-\frac{\partial \theta}{\partial x} = J\frac{\partial x}{\partial t}. \tag{13}$$

Here $J = L/(c_p(T_m - T_w)$ is a nondimensional latent heat (Stefan number). The exact solution at any time t is

$$\theta = \mathrm{erf}(x/2t^{1/2}))/\mathrm{erf}(\Lambda) - 1, \tag{14}$$

where Λ is the solution of the equation

$$\sqrt{\pi} \cdot \Lambda \exp(\Lambda^2)\,\mathrm{erf}(\Lambda) = 1/J. \tag{15}$$

The position of the interface is defined by

$$\delta(t) = 2\,\Lambda\,\sqrt{t}. \tag{16}$$

We solved this problem with our 2D approach using thermal insulation conditions for the side wall, which leads to a 1D solution with no y-dependence. We used values of J between 0.25 to 20, different meshes in the x direction (10 to 20 nodes) and time steps ranging from 0.01 to 0.1. The number of iterations of IFEM at each time step was not

TABLE I

Position of the Interface in Comparison to Analytical Solution

	Case $J = 0.25$		Case $J = 0.125$	
Time	Exact	Numer.	Exact	Numer.
0.01	0.1991	0.1991	0.2387	0.2387
0.02	0.2816	0.2814	0.3377	0.3359
0.03	0.3449	0.3449	0.4136	0.4115
0.04	0.3983	0.3984	0.4776	0.4754

more than four for convergence of the node locations (maximum node movement during iteration less than 10^{-4} and residual R less 10^{-6}). The results of our comparison are shown in Table I and Fig. 4. For the range of parameters considered, the difference between numerical and analytical values of the front location did not exceed 0.8%. This difference decreased with refinement of space and time discretization. A more sensitive measure of the agreement between the exact and numerical solution is shown in Fig. 4. Here we present a comparison of the exact heat flux at the interface with the heat flux obtained through numerical differentiation of the computed temperature field.

5. A PRACTICAL EXAMPLE

Here we present a computation using data from a directional solidification experiment with cadmium zinc telluride [31]. A melt and crystal are in contact and contained in an tapered ampoule (shown in Fig. 5). The crystal–melt interface is initially stationary and coexists with an initially stationary temperature profile also depicted in Fig. 5. The thermophysical properties for a cadmium zinc telluride

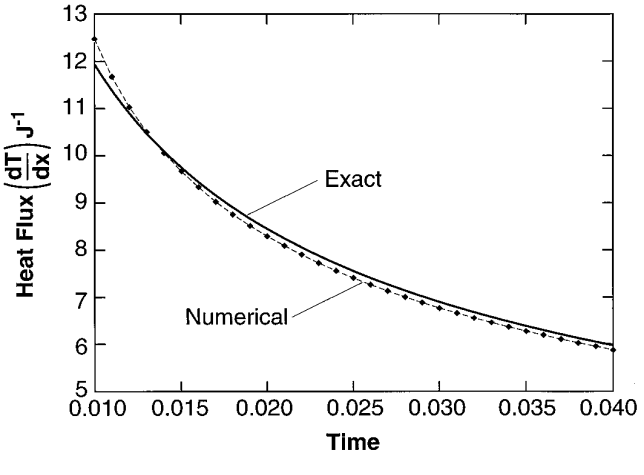

FIG. 4. Comparision of analytical and numerical values of dimensionless heat flux $(\partial T/\partial x)J^{-1}$ versus time, case $J = 0.125$.

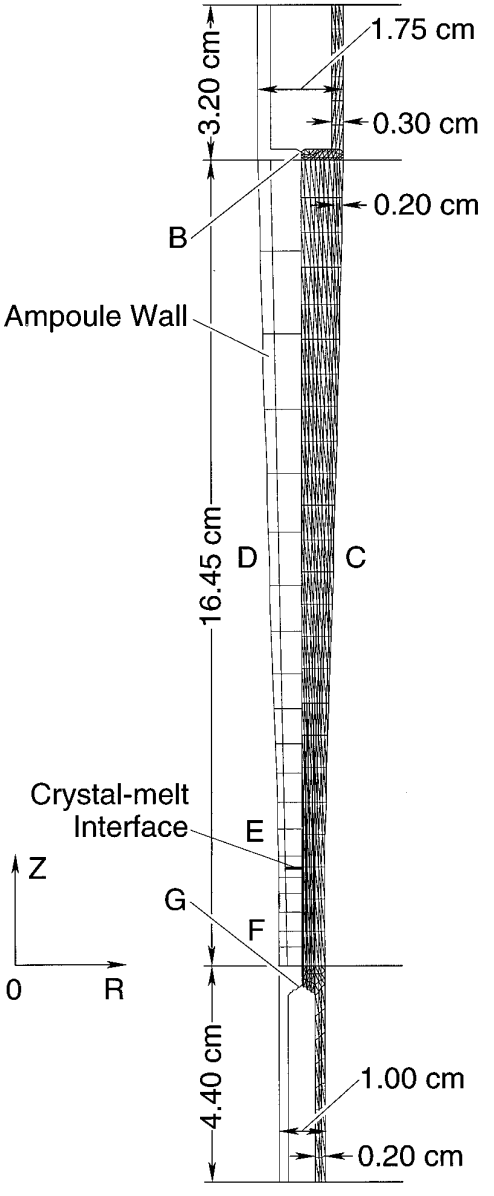

FIG. 5. The ampoule geometry showing the typical mesh for each subdomain and locations of the thermocouples B, C, D, E, F, and G.

crystal–melt system are listed in Table II. The ampoule properties were taken to be those of silica glass. The zinc is dilute in the case under investigation and the properties of the phase diagram enable us to assume a constant melting temperature. For $t > 0$, directional solidification of the crystal takes place as the boundary temperatures are changed systematically to advance the melting isotherm, T_M, toward the initially "hot-end" of the ampoule. The temporal and spatial boundary temperature profiles (see Fig. 6) used in the calculation were obtained from experimental measurements [31]. These measurements were interpolated to obtain a set of values used for T_{ex} in (3) at

TABLE II

Properties of ZnCdTe Used in Computations

Property	Value	Units
Thermal conductivity (melt)	0.018	$W \cdot cm^{-1} \cdot K^{-1}$
Thermal conductivity (crystal)	0.009	$W \cdot cm^{-1} \cdot K^{-1}$
Thermal conductivity (ampoule)	0.29	$W \cdot cm^{-1} \cdot K^{-1}$
Density (crystal and melt)	6.2	$g \cdot cm^{-3}$
Latent heat L	210	$J \cdot g^{-1}$
Heat capacity (crystal and melt)	0.29	$J \cdot g^{-1} \cdot K^{-1}$

all points on the ampoule boundary. Figure 7 shows the computed position and shape of the interface at equally spaced time intervals. Initially the interface was flat. Solidification then takes place rapidly and the interface develops a deeply curved profile. At later times the solidification velocity decreases and the interface gradually flattens although it retains a weakly curved shape. Table III gives typical performance characteristics of the IFEM method for this problem.

6. SOLIDIFICATION OF A BINARY ALLOY

In this section we consider the directional solidification of a binary alloy and account for species diffusion in both the melt and crystal during solidification. Species transport by diffusion is governed by the diffusion equation

$$\frac{\partial c}{\partial t} = \nabla(D \nabla c), \tag{15}$$

which is satisfied in each phase. Species diffusion through the ampoule wall is proscribed, i.e.,

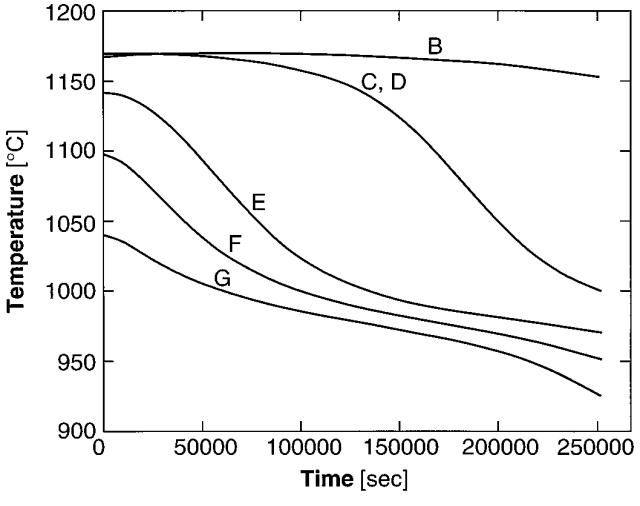

FIG. 6. Temperature versus time for thermocouples B, C, D, E, F, and G of Fig. 5.

$$D_{m,c} \frac{\partial c}{\partial n} = 0, \tag{16}$$

at the ampoule walls and conservation of mass at the interface is guaranteed by

$$-D_{\mathrm{m}} \boldsymbol{n} \cdot \nabla c_{\mathrm{m}} + D_{\mathrm{c}} \boldsymbol{n} \cdot \nabla c_{\mathrm{c}} = \boldsymbol{V} \cdot \boldsymbol{n} (c_{\mathrm{m}} - c_{\mathrm{c}}), \tag{17}$$

at the crystal–melt interface and c_{m}, c_{c}, D_{m}, D_{c} are the melt, crystal species concentration, and the melt crystal species diffusivities, respectively. $\boldsymbol{V}$ and $\boldsymbol{n}$ are, respectively, the node velocity and the unit normal vector at the crystal–melt interface. For a two-component solid solution, the equilibrium phase diagram yields the relation

$$c_{\mathrm{c}} = k(c_{\mathrm{m}}) c_{\mathrm{m}} \tag{18}$$

which, for this paper, we assume holds away from equilibrium and is used together with (17) to complete the formulation. The initial value of species concentration in the whole region is $c(\boldsymbol{x}, t_0) = c_0(\boldsymbol{x})$, where $\boldsymbol{x} = (x, y)$ or (r, z) in 2D-Cartesian and cylindrical coordinate systems, respectively. Recall (from Fig. 2) that solidification takes place along the z-coordinate.

The interface front velocity is determined from the solution of the thermal problem. The only coupling between thermal and mass transfer occurs through the dependence of the melting temperature on species concentration.

A finite-element approach has been used for the solution of the problem. The concentration field is approximated by

$$c = \sum_{i=1}^{N_c} c^i \Phi^i(x) \equiv c^i \Phi^i(x), \tag{19}$$

where $c^i(t)$ are the nodal values of concentration and other terms are the same as in (6). As in the previous problem, a Galerkin formulation is used to find the unknown c^i. The Galerkin equations for (15) are

$$\int_{\boldsymbol{G}} \left(\frac{\partial c}{\partial t} \Phi^i - \boldsymbol{V} \cdot \nabla c \, \Phi^i + D \nabla c \cdot \nabla \Phi^i \right) dG - \int_{\boldsymbol{S}_i} D \frac{\partial c}{\partial n} \Phi^i \, dS = 0, \tag{20}$$

where the second surface integral carried out on the phase interface S_{m} only and vanishes at the ampoule boundary due to (16). An additional convective term containing the product of $\boldsymbol{V}$ and the concentration gradient appears due to the mesh advection.

Using (19) yields the following system to be solved for the unknown c_i

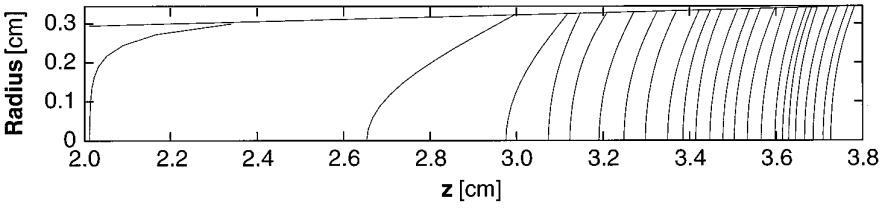

FIG. 7. Interface location and shape at different times.

$$\int_G \left(\frac{\partial c^j}{\partial t} \Phi^j \Phi^i - \boldsymbol{V} \cdot c^j \nabla \Phi^j \Phi^i + D c^j \nabla \Phi^j \cdot \nabla \Phi^i \right) dG - \int_{S_i} D \frac{\partial c}{\partial n} \Phi^i \, dS = 0. \tag{21}$$

Time discretization is again provided by finite differences:

$$\frac{\partial c}{\partial t} = (c(x, t + \tau) - c(x, t))/\tau. \tag{22}$$

The interface S_m between the melt and crystal is characterized by the difference in species diffusivities D_c, D_m in species concentration between the crystal and the melt. To describe this we use two unknowns, c_c and c_m, for each of the interface nodes. The two corresponding equations at these nodes are then (18) and (21) with the boundary integral computed according to (17).

Numerical experiments for mass diffusion have been undertaken for few cases for different values of k in (18), including regular diffusion through a moving interface, when $k = 1$, as well as $k < 1$ and $k > 1$. All other coefficients are set to unity.

In all these cases, the initial position of the interface was at $Z = L/4$ where $L = 20$. The initial temperature field changed linearly from $T = -1$ at the cold end to $T = 0$ (melting temperature) at the interface and then to $T = 1$, the boundary condition at the hot end. The nondimensional thermal conductivity throughout the domain is $\lambda = 1$, and the diffusivities are $D_m, D_c = 1$. As the melt–crystal interface asymptotically moves to the steady position at the midplane of the domain with time, the evolution of the temperature field and the position of the interface and species concentration was computed according to the algorithms described in this and the previous sections. Selected examples are discussed below.

TABLE III

Algorithm Performance for the Example Given in Fig. 5

Computer	SGI Indigo 50 Mhz
Number of nodes/elements	570/1036
Solver	Direct, Frontal [34]
Number of Newton iterations (to reach a relative accuracy of 10^{-5})	3–5
Number of mesh smoothing iterations	5
Time step value	100 to 10^4 s
Total CPU time per time step	4–7 s

For $k = 1$ the solution obtained by our IFEM method is compared with the FEM solution for the diffusion problem. Figure 8 shows profiles of the concentration at different times. The initial step in species concentration, $c_{0c} = 0.5$ at the left side of the interface and $c_{0m} = 1$ at the right one at time $t = 0$ decays with a time. The instantaneous location of the moving interface is marked by the symbol "*." When $k = 1$, as it is here, there is no dependence of concentration on the velocity of the interface. The solution must be the same as in a stationary domain. The solution in the same domain was also obtained by regular FEM on a static mesh (circles) and is provided for comparison in Fig. 8. The discrepancy was small enough (less than 0.1 to 1%). One can see that relation (17) holds exactly for both methods.

Results for the last two cases ($k < 1$ and $k > 1$) are

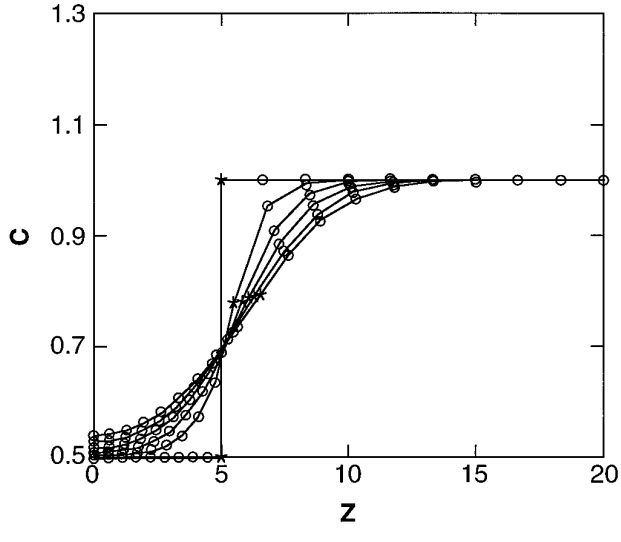

FIG. 8. Evolution of concentration profiles from an initial step for $k = 1$.

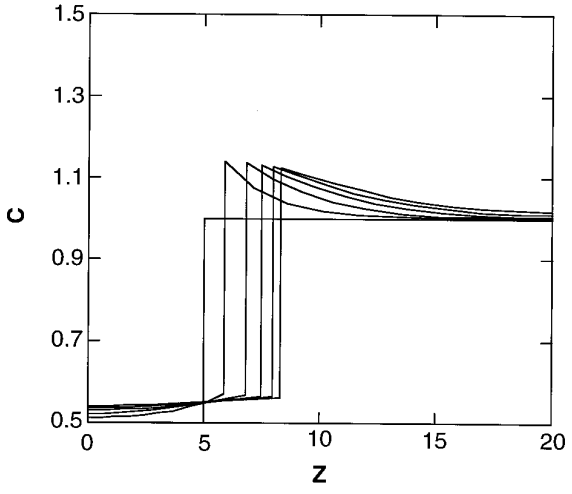

FIG. 9. Evolution of concentration profiles from initial step for $k = 0.5$.

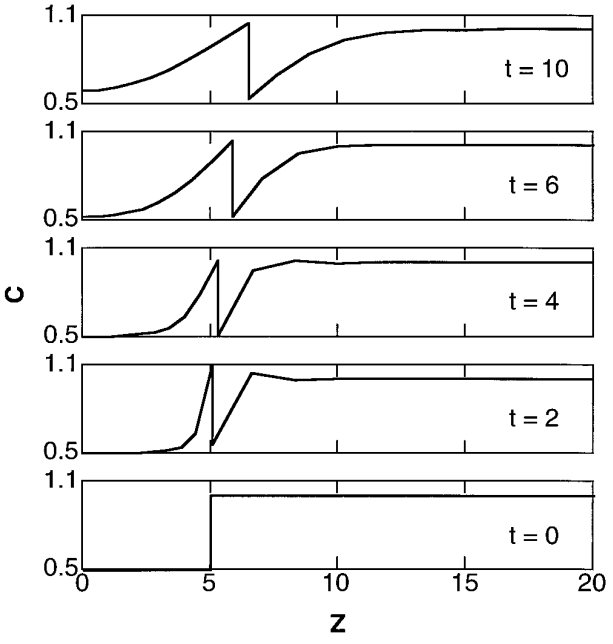

FIG. 11. Evolution of the concentration profile for solidification of an initially uniform melt ($c = 1.0$) and initially uniform crystal ($c = 0.5$), $k = 2$.

presented in Figs. 9–11. The triangles in Fig. 10 represent the comparison with a simplified 1D model, which was presented in [32] for the case when diffusion in the crystal is neglected. From the computed profiles one can see that relation (17) holds exactly, and the concentration jumps at the interface by an amount given by the distribution coefficient k, and is otherwise smooth in the crystal and in the melt, even though the mesh is rather coarse.

Figure 11 presents the case for $k = 2$, when the initial concentration field did not satisfy (17). The evolution of the concentration profile demonstrates how this initial condition influences the evolution of the concentration field. Condition (17) is enforced at the first step by the algorithm described above.

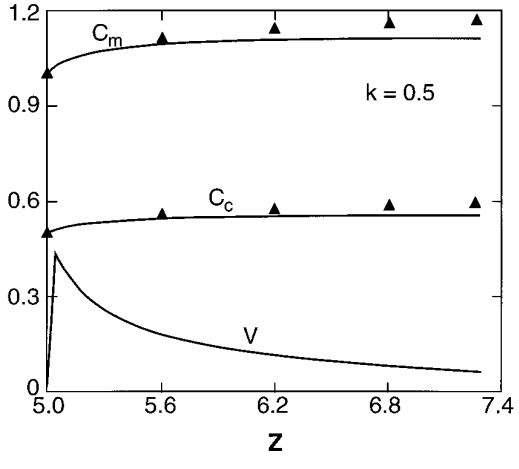

FIG. 10. Evolution of the radially averaged solidification velocity and concentration at the interface versus interface location, $k = 0.5$; triangles present results by using approach [32].

Figure 12 shows the convergence history for an axisymmetric temperature field and mesh starting with the initial guess shown in Fig. 12a. Here the initial guess has an interface which is tilted down toward the centerline. The dimensionless temperatures are 1 and -1 at the top and bottom, and the ampoule wall is adiabatic. The final position of the interface should be at $z = 0.5$ ($T_m(r, 0.5) = 0$) and the solution converges to this in a few iterations, see Fig. 12b. Figure 13 shows the same problem but for two different initial guesses. The final state should be a simple temperature profile (linear in z). In Fig. 13a the first guess converges rapidly to the correct solution in three iterations. The temperature gradients in the vicinity of the zero isotherm near the walls (Fig. 13b) are vanishingly small and the first guess leads to a (locally) vanishingly small Jacobian (see Eq. (11)). The mesh degenerates and the solution diverges. For the examples presented in Figs. 12–13 no vertex averaging (smoothing) or temperature field updating (step 1.2, Section 3.) was carried out. Figure 14 shows the combined effects of these two procedures on the example discussed in Section 5 (the geometry has been compressed in the z-direction to highlight the differences in the meshes). With smoothing and temperature updating, the solution is obtained readily (Fig. 14a). In contrast, Fig. 14b shows that the mesh size varies abruptly and that elements are concentrated in the vicinity of the interface. Note especially the coarse, highly stretched elements in the solid. In this case the solution diverges rapidly.

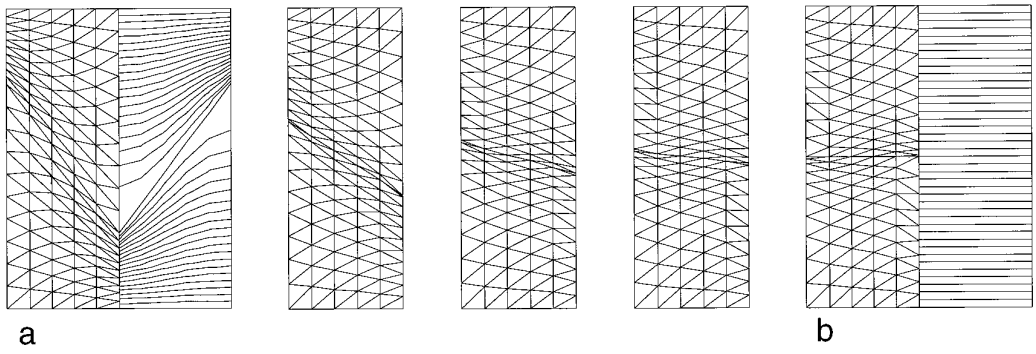

FIG. 12. Convergence history for an axisymmetric temperature field and mesh starting with the initial guess (a) to the exact solution (b).

7. CONCLUSIONS

This work confirms the suitability of the modified IFEM approach as an attractive alternative to other existing methods for treating moving boundary problems. The solution algorithms described here represent a significant modification to previous IFEM methods in that it allows for time-dependent and nonmonotonic thermal boundary conditions and two-component systems with liquid and solid state diffusion. The method can handle large distortions of the interface and can also be used for systems with internal heat sources provided that these do not lead to local temperature extrema. The algorithm and related software is being used to assist in the postflight analysis of the experimental data from cadmium zinc telluride crystal grown under low gravity conditions on the first and second U.S. Microgravity Laboratory (USML-1,2) [33].

APPENDIX: IFEM FORMULAE FOR 2D AND AXISYMMETRIC CASES WITH LINEAR TRIANGULAR ELEMENTS

The main step in the algorithm is a Newton iteration that updates the node positions to reduce the residual of equation (8) at each time step. That is,

$$R^i = \int_{\boldsymbol{G}} \left(\rho c_p \left(\frac{\partial u}{\partial t} - \boldsymbol{V} \nabla u \right) - \nabla(\lambda \nabla u) - Q \right) \Phi^i \, dG = 0. \tag{A.1}$$

The integral (A.1) is computed by a summation of the integrals over each element of the mesh, i.e., $R^i = \sum_l^{Ne} R_e^i$, where Ne is the total number of elements. For triangular elements the integral is readily computed using local area coordinates L_1, L_2, L_3, since local functions

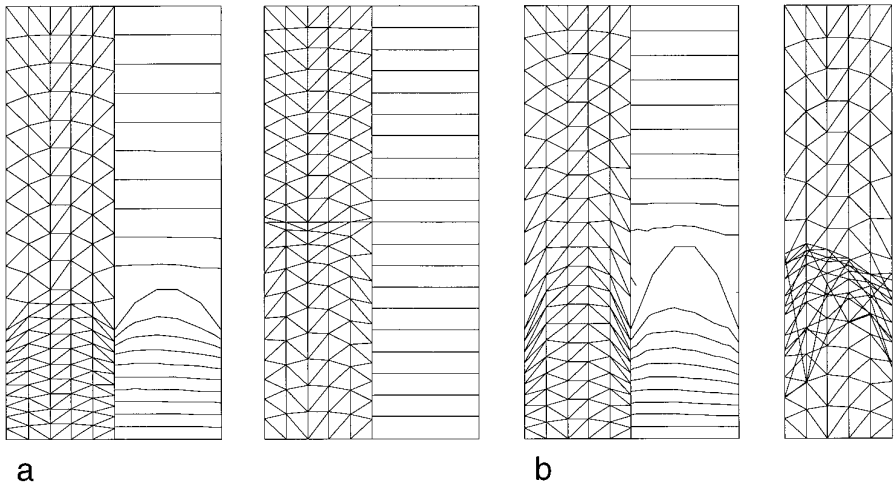

FIG. 13. Convergence for an axisymmetric temperature field and mesh starting with a poor initial guess; (a) convergence after 5 iterations; (b) divergence in 3 iterations.

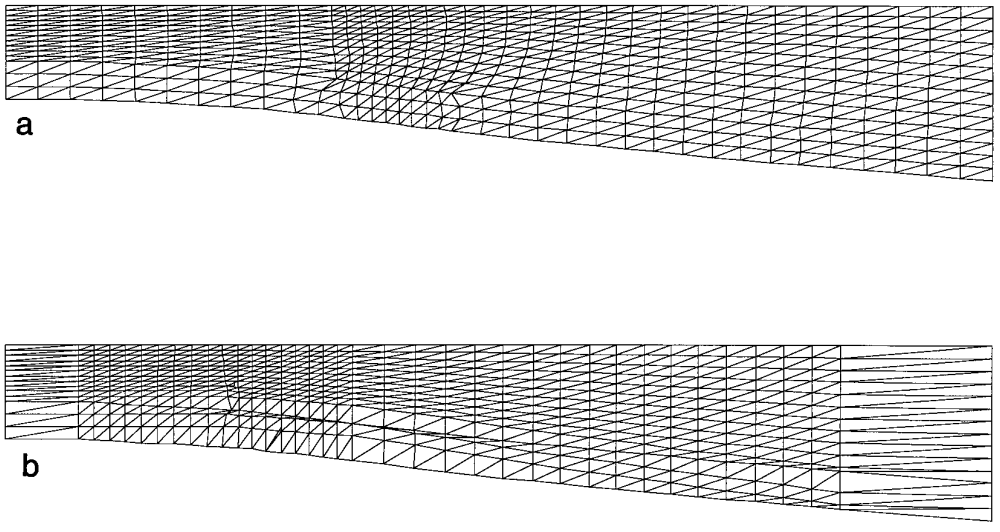

FIG. 14. Effect of smoothing and temperature updating: (a) typical mesh for transient problem from Fig. 5 for presented method; (b) mesh for original IFEM [25] before it fails (ends of ampoule are not shown and geometry is compressed in z-direction).

and their derivatives are expressed explicitly through local coordinates. Then after integrating (A.1) by parts we have

$$R_e^i = \int_{G_e} \left[\rho c_p \left(\frac{\partial u}{\partial t} \Phi^i - \boldsymbol{V} \nabla u \, \Phi^i \right) + \lambda \nabla u \nabla \Phi^i - Q \Phi^i \right] r \, \Delta \, dL_1 \, dL_2 \, dL_3 - \int_0^1 \lambda \frac{\partial u}{\partial n} \Phi^i \, S_e r ds, \tag{A.2}$$

where r is the radius for cylindrical coordinates or $r = 1$ for Cartesian coordinates, Δ is the Jacobian of transformation to local triangular coordinates and S_e is the length of an element side. S_e, is given by

$$S_e = \sqrt{(x_1 - x_k)^2 + (y_1 - y_k)^2}$$

where (x_j, y_j) are the coordinates of a triangle with side S_e on the boundary S_2.

The expression for the Jacobian of the residual on a triangle element with respect to the triangle coordinates x_j is

$$\begin{aligned} \frac{\partial R_e^i}{\partial x_j} = & \int_{G_e} \left(\rho c_p \left(\frac{\partial u}{\partial t} \Phi^i - \boldsymbol{V} \nabla u \, \Phi^i \right) + \lambda \nabla u \nabla \Phi^i - Q \, \Phi^i \right) \frac{\partial \Delta}{\partial x_j} \\ & + \left(-\rho C_p \left(V \cdot \frac{\partial}{\partial x_j} \nabla u + \frac{\partial V}{\partial X_j} \cdot \nabla u \right) \Phi^i + \lambda \nabla u \frac{\partial}{\partial x_j} \nabla \Phi^i \right. \\ & \left. + \lambda \frac{\partial}{\partial x_j} \nabla u \cdot \nabla \Phi^i + \frac{\partial Q}{\partial x_j} \Phi^i \right) \Delta \, r dL_1 dL_2 dL_3 \\ & - \int_0^1 \left(\frac{\partial}{\partial x_j} \left(\lambda \frac{\partial u}{\partial n} \right) S_e + \lambda \frac{\partial u}{\partial n} \frac{\partial S_e}{\partial x_j} \right) \Phi^i \, r \, ds. \end{aligned} \tag{A.3}$$

Since $dG = 2 \pi r \, dr \, dz$ for the (r, z) coordinate system, the multiplier r is present for the axisymmetric case. For the 2D Cartesian coordinate system, r is set equal to 1. A constant multiplier is omitted in all the terms. We assume for the simplicity, that only the z or x-coordinate is allowed to move.

In a local triangular coordinate system the following relationships are used for the transformation between local triangle area coordinates L_1, L_2, L_3 and the global Cartesian coordinates (x, y):

$$L_i = (A_i + B_i x + C_i y)/2\Delta$$

and

$$\begin{aligned} x &= L_1 x_1 + L_2 x_2 + L_3 x_3, \\ y &= L_1 y_1 + L_2 y_2 + L_3 y_3. \end{aligned} \tag{A.4}$$

Here (x_i, y_i), $i = 1, 2, 3$ are triangular vertex coordinates,

$$\Delta = 0.5 \, (y_1(x_2 - x_3) + y_2 (x_3 - x_1) + y_3(x_1 - x_2) \tag{A.5}$$

is a triangle area, and

$$\begin{aligned} A_1 &= x_2 y_3 - x_3 y_2, \\ A_2 &= x_3 y_1 - x_1 y_3, \\ A_3 &= x_1 y_2 - x_2 y_1, \\ B_1 &= y_2 - y_3, \\ B_2 &= y_3 - y_1, \\ B_3 &= y_1 - y_2, \\ C_1 &= x_3 - x_2, \\ C_2 &= x_1 - x_3, \\ C_3 &= x_2 - x_1. \end{aligned}$$

For a linear triangular element the basis functions $\Phi^i(x, y)$ are local area coordinates $L_i(x, y)$, so

$$u = u^k L_k(x, y), \quad \nabla u = u^k \nabla L_k. \tag{A.7}$$

The expressions for the terms under the integral over each element are

$$\frac{\partial \Delta}{\partial x_j} = \frac{1}{2} B_j,$$

$$\nabla \Phi^i = \nabla L_i = \frac{1}{2\Delta}(B_i, C_i),$$

$$\frac{\partial}{\partial x_j} \nabla \Phi^i = \frac{1}{4\Delta}\left(-\frac{B_i B_j}{\Delta}, -\frac{C_i B_j}{\Delta} + C_{ij}\right), \tag{A.8}$$

$$\text{where } C_{ij} = \frac{\partial C_i}{\partial x_j} = \begin{pmatrix} 0 & -1 & 1 \\ 1 & 0 & -1 \\ -1 & 1 & 0 \end{pmatrix},$$

$$\frac{\partial \nabla u}{\partial x_j} = u^k \cdot \frac{\partial \nabla \Phi^k}{\partial x_j},$$

where an implicit sum is assumed over repeated indices.

For the terms under the surface integral

$$\frac{\partial S_e}{\partial x_j} = \frac{x_j - x_k}{S_e}, \tag{A.9}$$

where x_j, x_k are the x-coordinates of a triangle side S_e lying at the boundary S_2.

The part of the Jacobian, related to the surface integral in (A.3) has the form

$$\frac{\partial R^i_{S_e}}{\partial x_j} = \int_0^1 \left(\frac{\partial}{\partial x_j}(\alpha(u^l \Phi^l - u_e)) S_e + \alpha(u^l \Phi^l - u_e) \frac{x_j - x_k}{S_e}\right) \Phi^i \, r \, ds \tag{A.10}$$

for the case of a convection heat exchange boundary condition, or

$$\frac{\partial R^i_{S_e}}{\partial x_j} = -\int_0^1 \left(\frac{\partial q}{\partial x_j} S_e + q \frac{x_j - x_k}{S_e}\right) \Phi^i \, r \, ds \tag{A.11}$$

for the case of the applied heat flux $\boldsymbol{q}$ at the element boundary S_e. The derivative of the first terms in (A.10) and (A.11) should be computed numerically since the dependencies α, u_e, and q on the coordinates are unknown *a priori*.

It is also important to note that:

(a) Anticlockwise triangle vertex numbering is strongly recommended. This ensures positive values of triangular areas and the correct signs of the Jacobian.

(b) For all the terms in the boundary integrals (A.2), (A.3), (A.10), (A.11) accurate Gauss integration is required to obtain stable quadratic convergence.

(c) A smoothed Newton technique is sometimes needed when the initial guess for the temperature and interface position are poor. This will accelerate convergence. The smoothing is implemented via

$$x_i^{n+1} = x_i^n \, a \cdot \left(\frac{\partial R^i}{\partial x_j}\right)^{-1} R^j(x^n), \tag{A.12}$$

where $0 < a < 1.0$. Typically, we use the value of $a = 0.5$.

ACKNOWLEDGMENTS

Support of this work by the National Aeronautics and Space Administration under Grant NAG 8-790, and by the Northrop–Grumman Corporate Research Center (Dr. David Larson, PI, SUNY, Stonybrook) is gratefully acknowledged. Thanks are also due to Franz Rosenberger for careful perusal of the manuscript.

REFERENCES

1. R. A. Brown, *AICHE J.* **34,** 881 (1985).
2. H. M. Ettouney and R. A. Brown, *J. Comput. Phys.* **49,** 118 (1983).
3. J. J. Derby and R. A. Brown, *J. Electroch. Soc. Solid-State Sci. Technol.* **132,** 470 (1985).
4. C. Cuvelier and J. M. Dressen, *J. Fluid Mech.* **169,** 1 (1986).
5. G. Chen and B. Roux, "Heat Transfer, Thermocapillary Convection and Interface Shapes in Floating Zone Crystal Growth with a Magnetic Field," in *Proceedings, IAC'94 Int. Aerospace Congress, August* 15–19, 1994, *Moscow, Russia, AIAA J.,* to appear.
6. Y. Zhang, J. I. D. Alexander, and J. Ouazzani, *Int. J. Num. Methods Heat Fluid Flow* **4,** 115 (1994).
7. J. M. Floryan, Appl. Mech. Rev. **42,** 323 (1989).
8. K. Tsiveriotis and R. A. Brown, *Int. J. Num. Methods Fluids* **16,** 827 (1993).
9. M. E. Rose, *Math. Comput.* **4,** 249 (1960).
10. V. R. Voller and M. Gross, *Int. J. Heat Mass Transfer* **24,** 545 (1981).
11. V. R. Voller, *Appl. Math. Modeling* **11,** 110 (1986).
12. W. D. Bennon and F. P. Incropera, *Int. J. Heat Mass Transfer* **30,** 2171 (1987).
13. V. Alexiades, *Quart. Appl. Math.* **63,** 143 (1985).
14. A. B. Crowley and J. R. Ockendon, *Int. J. Heat Mass Transfer* **22,** 941 (1979).
15. A. A. Wheeler, W. J. Boettinger, and G. B. Mcfadden, *Phys. Rev. A* **45,** 7424 (1992).
16. B. I. Halperin, P. C. Hohenburg, and S. K. Ma, *Phys. Rev. B* **10,** 139 (1974).
17. J. S. Langer, *Directions In Condensed Matter Physics* (World Scientific, Singapore, 1986), p. 164.

18. G. Caginalp, *Arch. Rat. Mech. Anal.* **92,** 505 (1986).
19. J. Smith, *J. Comput. Phys.* **39,** 112 (1981).
20. A. A. Wheeler, B. T. Murray, and R. J. Schaefer, *Phys. Rev. D* **66,** 243 (1993).
21. S.-L. Wang, R. F. Sekerka, A. A. Wheeler, B. T. Murray, S. R. Coriell, R. J. Braun, and G. B. Mcfadden, *Phys. Rev. D* **69,** 189 (1993).
22. G. E. Bell, ''Inverse Formulation as a Method For Solving Certain Melting and Freezing Problems,'' in *Numerical Methods in Heat Transfer, Vol. 3,* edited by R. W. Lewis (Wiley, New York, 1985).
23. N. M. Tsirelman, *Int. J. Heat Mass Transfer* **35,** 2983 (1992).
24. N. M. Tsirelman, *Int. J. Heat Mass Transfer* **35,** 2997 (1992).
25. A. N. Alexandrou, *Int. J. Numer. Methods Eng.* **28,** 2383 (1989); **36,** 135 (1993).
26. P. M. Adornato and R. A. Brown, *J. Cryst. Growth* **80,** 155 (1987).
27. D. H. Kim, *Dynamic Analysis of Transport Phenomena in Directional Solidification of Binary Alloys,* Ph.D. thesis, MIT, 1990.
28. J. F. Nye, *Physical Properties of Crystals* (Oxford Univ. Press, London, 1972).
29. J. F. Thompson, Z. U. A. Wausi, and C. W. Mastin, *Numerical Grid Generation* (North-Holland, New York, 1985).
30. S. A. Cannan, M. B. Stephenson, and T. Blacker, *Finite Elements Anal. Design* **13** (1993), 185–190.
31. D. J. Larson, Gruman Corporate Research Center, personal communication.
32. J. C. Clayton, M. C. Davidson, D. C. Gilles, and S. L. Lehoczky, *J. Cryst. Growth* **60,** 373 (1982).
33. D. J. Larson, J. I. D. Alexander, D. C. Gilles, F. M. Carlson, J. Wu, and D. Black, *Orbital Processing of High Quality CdTe Compound Semiconductors,* NASA Conference Publication 3272, Vol. 1, May 1994 (unpublished).
34. V. I. Polezhaev, A. I. Prostomolotov, and A. I. Fedoseyev, Finite element method in viscous fluid mechanics problems (a review), in *Advances in Science and Technology,* Fluid Mechanics Series Vol. **21,** p. 3 (VINITI, Moscow, 1987); (see also Hemisphere, *Soviet Rev. Appl. Mech.* **3** (1990).